Modulation of RNA-binding properties of the RNA helicase UPF1 by its activator UPF2

GUANGPU XUE,[1] VINCENT D. MACIEJ,[1] ALEXANDRINA MACHADO DE AMORIM,[1] MELIS PAK,[1] UMA JAYACHANDRAN,[2,3] and SUTAPA CHAKRABARTI[1]

[1]Institute of Chemistry and Biochemistry, Freie Universität Berlin, D-14195 Berlin, Germany
[2]Max Planck Institute of Biochemistry, Structural Cell Biology Department, D-82152 Martinsried, Germany

ABSTRACT

The NMD helicase UPF1 is a prototype of the superfamily 1 (SF1) of RNA helicases that bind RNA with high affinity and translocate on it in an ATP-dependent manner. Previous studies showed that UPF1 has a low basal catalytic activity that is greatly enhanced upon binding of its interaction partner, UPF2. Activation of UPF1 by UPF2 entails a large conformational change that switches the helicase from an RNA-clamping mode to an RNA-unwinding mode. The ability of UPF1 to bind RNA was expected to be unaffected by this activation mechanism. Here we show, using a combination of biochemical and biophysical methods, that binding of UPF2 to UPF1 drastically reduces the affinity of UPF1 for RNA, leading to a release of the bound RNA. Although UPF2 is capable of binding RNA in vitro, our results suggest that dissociation of the UPF1–RNA complex is not a consequence of direct competition in RNA binding but rather an allosteric effect that is likely mediated by the conformational change in UPF1 that is induced upon binding its activator. We discuss these results in light of transient interactions forged during mRNP assembly, particularly in the UPF1-dependent mRNA decay pathways.

Keywords: RNA helicase; allosteric modulator; dynamic mRNP

INTRODUCTION

The coat of proteins that assemble on a messenger RNA (mRNA), leading to the formation of a messenger ribonucleoprotein (mRNP), represents a major class of effectors of post-transcriptional gene regulation (Gehring et al. 2017). Messenger RNPs are often transient in nature and undergo rapid assembly and disassembly depending on the functional requirement of the cell. A class of proteins that mediate remodeling while being an integral part of mRNPs themselves are RNA helicases. These enzymes are molecular motors that harness the energy of ATP binding and hydrolysis to bring about conformational changes in RNA, which facilitate binding of some protein factors while preventing others from associating with the RNA. RNA helicases can also mediate protein–protein interactions, often acting as scaffolds for mRNP assembly (Linder and Jankowsky 2011; Bourgeois et al. 2016; Machado de Amorim and Chakrabarti 2021).

The RNA helicase Up-Frameshift1 (UPF1) is a central effector of the nonsense-mediated mRNA decay (NMD) pathway and has diverse functions, ranging from target selection in the early stages of the pathway to mRNP remodeling and recruitment of additional protein factors in the later stages of NMD (Leeds et al. 1991; Ohnishi et al. 2003; Okada-Katsuhata et al. 2012; Lee et al. 2015). The catalytic activity of UPF1 is greatly enhanced upon binding to a core NMD factor UPF2. UPF2 associates with another conserved NMD protein UPF3 to serve as an adaptor that connects the helicase to the exon-junction complex (EJC) (Chamieh et al. 2008; Buchwald et al. 2010). UPF1 is a multidomain protein, consisting of a *cis*-inhibitory cysteine-histidine rich (CH) domain and a helicase core comprising two RecA-like domains and two auxiliary domains, 1B and 1C (Fig. 1A; Cheng et al. 2007; Chamieh et al. 2008). The RecA-like domains together make up a deep cleft for ATP binding and on the opposite side, a shallow surface which allows RNA to bind across it. UPF1 spans 9–11 nt on single-stranded RNA and binds with a high affinity of ~50 nM (Chakrabarti et al. 2011). The basal catalytic activity of UPF1 is repressed owing to clamping down of the auxiliary domain 1B on the 3′-end of the RNA. The clamp is

[3]**Present address:** Wellcome Trust Centre for Cell Biology, University of Edinburgh, Edinburgh EH9 3BF, United Kingdom
Corresponding author: chakraba@zedat.fu-berlin.de
Article is online at http://www.rnajournal.org/cgi/doi/10.1261/rna.079188.122.

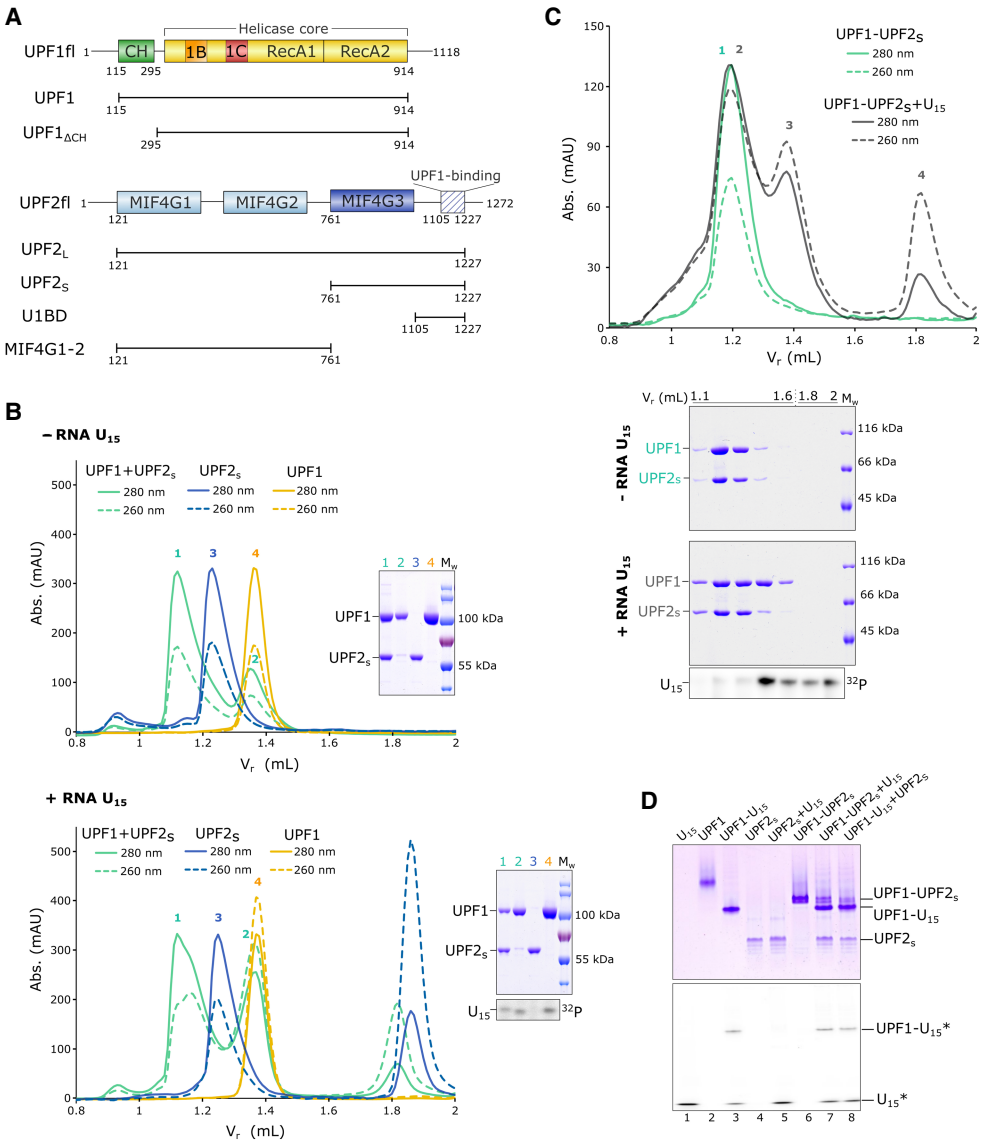

FIGURE 1. UPF1 does not form a stable ternary complex with UPF2 and RNA in vitro. (*A*) Schematic of the domain organizations of UPF1 and UPF2. The helicase core comprising the RecA1 and RecA2 domains is colored yellow. The CH domain and auxiliary domains 1*B* and 1*C* are shown in green, orange and red, respectively. The MIF4G domains of UPF2 are in shades of blue, while the partially disordered UPF1-binding domain (U1BD) is denoted as a hatched box. The constructs used in this study are represented by black lines *under* the respective proteins. (*B*) Analytical SEC and corresponding SDS-PAGE analyses of mixtures of UPF1 and UPF2$_S$, in the absence (*top* panel) and presence of U$_{15}$ RNA (*bottom* panel). SEC runs of individual UPF1 and UPF2$_S$ in the absence and presence of U$_{15}$ RNA have been included for comparison. (*Left*) Overlay of chromatograms of the UPF1–UPF2$_S$ mixtures (green traces), UPF1 alone (yellow traces) and UPF2$_S$ alone (blue traces). In this and all other figures for SEC analysis, solid and dashed lines denote absorbances at 280 and 260 nm, respectively. (*Right*) Corresponding PAGE analyses of the peak fractions of each run. In addition to SDS-PAGE for visualizing proteins, the *bottom* panel includes a urea-PAGE analysis of the radiolabeled peak fractions to detect U$_{15}$ RNA. An SDS-PAGE analysis of consecutive fractions of the *bottom* panel is shown in Supplemental Figure 1A. Addition of U$_{15}$ RNA to a mixture of UPF1 and UPF2$_S$ does not result in a detectable amount of RNA-bound UPF1–UPF2 complex, but rather promotes dissociation of the UPF1–UPF2 complex, resulting in free UPF2$_S$, which leads to a broader peak 1, and free UPF1 that binds the U$_{15}$ RNA. (*C*) Analytical SEC analysis of a mixture of a UPF1–UPF2$_S$ complex and U$_{15}$ RNA. (*Top*) Overlay of chromatograms of the preformed UPF1–UPF2$_S$ complex (green traces) and the same complex with U$_{15}$ RNA added (black traces). (*Bottom*) SDS- and urea-PAGE analyses of consecutive SEC fractions in order of increasing retention volume, as indicated. Detection of U$_{15}$ RNA is as described above. Addition of RNA to a stable UPF1–UPF2$_S$ complex leads to partial dissociation of the protein complex instead of formation of a stable ternary complex with RNA. The peak between 1.8 and 2 mL in *B* and *C* corresponds to excess U$_{15}$ RNA. (*D*) Native PAGE analysis of a UPF1–UPF2$_S$ complex in the absence and presence of fluorescein-labeled U$_{15}$ RNA, and a UPF1–U$_{15}$ RNA complex in the absence and presence of UPF2$_S$. The individual UPF1 and UPF2 proteins as well as the UPF1–UPF2$_S$ and UPF1–U$_{15}$ complexes serve as markers for migration of the protein and RNA components on the native gel. Proteins are visualized by staining with Coomassie brilliant blue (*top* panel), and the U$_{15}$ RNA is detected by fluorescence scanning (*bottom* panel). Asterisks denote the fluorescein label. In solution, UPF1, UPF2$_S$, and U$_{15}$ RNA always partition into two binary complexes, UPF1–UPF2$_S$ and UPF1–U$_{15}$ RNA. As with analytical SEC (Fig. 1C), no ternary UPF1–UPF2$_S$–U$_{15}$ complex is detected in these conditions.

positioned indirectly by the CH domain, which interacts with the RecA2 domain to hold the helicase in an inactive conformation. Activation of UPF1 is due to a large conformational change in the helicase that is brought about upon binding of UPF2 to the CH domain (Clerici et al. 2009; Chakrabarti et al. 2011).

UPF2 is also a multidomain protein consisting of three MIF4G (middle of eIF4G) domains and a predominantly unstructured carboxy-terminal tail (Fig. 1A; Clerici et al. 2009, 2014). The third MIF4G domain (MIF4G3) has been shown to bind a number of proteins involved in different aspects of mRNA processing (such as UPF3, SMG1, Stau1, and the eukaryotic release factor eRF3), while the UPF1-binding region (U1BD, see also Fig. 1A) resides within amino acids 1105 to 1227 (Kadlec et al. 2004; Clerici et al. 2009, 2014; Lopez-Perrote et al. 2016; Gowravaram et al. 2019). The X-ray crystal structure of the UPF1–UPF2 complex shows that the composite U1BD of UPF2 is made up of two distinct secondary structural elements, an α-helix and a β-hairpin, which engage opposite surfaces of the UPF1-CH domain. In-solution NMR studies suggest that the β-hairpin structure is only adopted upon binding to UPF1, indicating that UPF2 also undergoes conformational changes in this process (Clerici et al. 2009). Although the available crystal structures of UPF1 bound to RNA and that of a UPF1–UPF2 complex allow insights into activation of UPF1 by UPF2, no experimental structure of a UPF1–UPF2–RNA ternary complex has been determined as yet. As such, our knowledge of assembly of the mRNP that leads to UPF1 activation remains incomplete.

In this study, we investigated the interactions of UPF1, UPF2, and RNA in vitro, with an aim to elucidate the mechanism of assembly of the mRNP that leads to UPF1 activation. To our surprise, we found that UPF1 cannot stably associate with UPF2 in the presence of RNA. Addition of RNA partially dissociates the UPF1–UPF2 complex; conversely, addition of UPF2 releases UPF1 from RNA to a great extent. Previous studies by Chamieh and coauthors also detected a decrease in binding of UPF1 to RNA in the presence of UPF2 and UPF3 (Chamieh et al. 2008). Although not apparent from the X-ray crystal structures of RNA-bound UPF1 and the UPF1–UPF2 complex, these observations suggest that the dynamics of RNA-bound UPF1 do not support its stable interaction with UPF2, and vice versa. We present here evidence to suggest that the interference of UPF2 on RNA binding by UPF1 is not due to direct competition between the two proteins for RNA but rather indirect effects brought about by conformational changes upon protein–protein/RNA interactions.

RESULTS AND DISCUSSION

The proteins UPF1 and UPF2 have a high binding affinity and readily form a stable complex in solution. We reconstituted a UPF1–UPF2 complex using a construct of UPF1 comprising its CH and helicase domains (referred to hereafter as UPF1, Fig. 1A) and a short UPF2 construct encompassing only its MIF4G3 and U1BD domains ($UPF2_S$) by mixing these two proteins in a molar ratio of 1.2:1, with a slight excess of UPF1 to favor complex formation. Analytical size-exclusion chromatography (SEC) was used to assess formation of a stable complex. SEC analysis of the UPF1–$UPF2_S$ protein mixture yielded two peaks, a major peak corresponding to the UPF1–$UPF2_S$ complex and a smaller peak of the excess UPF1 (Fig. 1B, top panel, green traces, and lanes 1 and 2 of the corresponding SDS-PAGE analysis of peak fractions). As a comparison, SEC runs were also performed with UPF1 and $UPF2_S$ alone (yellow and blue traces, respectively). To obtain a ternary complex of UPF1, UPF2, and RNA, we added a 15-mer polyuridine RNA (U_{15}) to the UPF1–$UPF2_S$ mixture and resolved the protein–RNA mixture by analytical SEC (Fig. 1B, bottom panel, green traces). We observed a prominent peak for UPF1 bound to RNA, as indicated by the higher absorbance of the peak fractions at 260 nm than at 280 nm (Fig. 1B, bottom panel, compare peaks and lanes 2 and 4 of SEC and SDS-PAGE analyses) and a broader, asymmetrical peak at approximately the same retention volume as the UPF1–$UPF2_S$ complex (Fig. 1B, compare peak 1 of top and bottom panels). SDS-PAGE analysis of continuous fractions of this SEC run suggested that the broad peak is an overlap of the peaks of the UPF1–$UPF2_S$ complex and $UPF2_S$ alone (Supplemental Fig. 1A). Notably, the lower absorbance at 260 nm than at 280 nm indicated that RNA is not stably associated with the UPF1–$UPF2_S$ complex (although a small amount of U_{15} RNA is detected in lane 1, corresponding to the peak 1 fraction of the urea-PAGE, Fig. 1B, bottom panel). The peak at 1.9 mL with a higher absorbance at 260 nm than at 280 nm corresponds to excess U_{15} RNA. In the presence of U_{15}, not all UPF1 formed a complex with UPF2; some preferentially associated with RNA. SDS-PAGE analyses of the SEC peak fractions of the UPF1/$UPF2_S$/RNA mixture and UPF1/$UPF2_S$ alone showed that less UPF1–$UPF2_S$ complex was formed in the presence of RNA, leaving more UPF1 free to associate with the U_{15} RNA (Fig. 1B, compare lane 1 of top and bottom panels).

To ascertain that the inability to isolate a stable UPF1–UPF2–RNA complex was not due to the experimental conditions in which the reconstitution was carried out, we performed analytical SEC with a preformed UPF1–$UPF2_S$ complex (isolated by preparative SEC) to which an equimolar amount of U_{15} RNA was added. Instead of a single peak for a UPF1–$UPF2_S$–RNA ternary complex, we observed two distinct peaks, one corresponding to UPF1–$UPF2_S$ and the other to a UPF1–RNA complex (Fig. 1C, peaks 2 and 3, and corresponding PAGE analyses). A similar observation was made with the UPF1–$UPF2_L$ complex that contains a near-full length construct of UPF2 encompassing all three MIF4G domains in addition to the U1BD (Supplemental Fig. 1B). We thus infer that addition of U_{15} RNA leads to

partial dissociation of the UPF1–UPF2 complex, following which UPF1 binds to RNA.

To corroborate our observations from analytical SEC assays, we performed a native gel analysis using reconstituted complexes of UPF1–RNA (fluorescein-labeled U_{15}) and UPF1–$UPF2_S$ (Fig. 1D, lanes 3 and 6, respectively). Addition of labeled U_{15} RNA to the UPF1–$UPF2_S$ complex led to partial release of $UPF2_S$ and formation of a UPF1–U_{15} complex. On the other hand, addition of $UPF2_S$ to the UPF1–RNA complex led to partial dissociation of UPF1 from the protein–RNA complex and formation of a UPF1–$UPF2_S$ complex (Fig. 1D, lanes 7 and 8, respectively). Also, an electrophoretic mobility shift assay (EMSA) of increasing concentrations of the UPF1–$UPF2_L$ complex with a radiolabeled U_{15} RNA showed appearance of a predominant shifted band corresponding to a UPF1–U_{15} complex and a weaker band corresponding to a $UPF2_L$–U_{15} complex. No super-shifted band corresponding to a ternary UPF1–$UPF2_L$–U_{15} complex was obtained (Supplemental Fig. 1C). Taken together, our observations clearly show that a stable complex of UPF1, UPF2, and RNA cannot be reconstituted in vitro. It is interesting that addition of RNA or UPF2 did not lead to complete dissociation of the UPF1–UPF2 or UPF1–RNA complexes, suggesting a dynamic equilibrium among the components and the interactions they engage in solution.

In cells, UPF1 is ~10-fold more abundant than UPF2 and can bind along the length of an mRNA transcript (Hein et al. 2015; Cho et al. 2022). A cryo-EM structure of the EJC–UPF3–UPF2–UPF1 complex shows UPF1 positioned toward the 3′-end of the EJC-bound RNA (Melero et al. 2012). However, UPF1 was also shown to be involved in NMD target selection, using its ATPase activity to discriminate between target and nontarget mRNAs (Lee et al. 2015). This step presumably occurs directly at or in close proximity of the premature termination codon (PTC), upstream of the EJC, where the translating ribosome is stalled. It is possible that binding of UPF2 temporarily displaces UPF1 from RNA and repositions it downstream from the EJC to remodel the 3′-end of the mRNP. To gain deeper insights into displacement of UPF1 from RNA by UPF2, we performed fluorescence anisotropy assays at pH 7.5, where increasing amounts of $UPF2_S$ were titrated into a mixture of UPF1 and U_{12} RNA that was labeled with 6-FAM at its 5′-end. The titration of $UPF2_S$ into the UPF1–RNA mixture was carried out in the absence of nucleotides. As expected, the UPF1–RNA mixture alone showed high fluorescence anisotropy. Increasing $UPF2_S$ concentrations led to a decrease in fluorescence anisotropy, which can be attributed to release of UPF1 from the labeled RNA (Fig. 2A). An identical trend in fluorescence anisotropy was observed at pH 6.5, where the catalytic activity of the UPF1–$UPF2_S$ complex is at its highest (Supplemental Fig. 2A,B). Interestingly, the fluorescence anisotropy at the highest concentrations of $UPF2_S$ tested did not go down to 0 (the value corresponding to free RNA in solution) but plateaued off at a relative value of 0.23, suggesting that some UPF1 remained bound to the RNA. This is in accordance with our observations from native PAGE analysis (Fig. 1D), where addition of $UPF2_S$ did not result in complete dissociation of the UPF1–RNA complex.

We next tested if the release of UPF1 from RNA in the presence of UPF2 is a consequence of direct competition for RNA binding. Although previous studies demonstrated binding of UPF2 to RNA, the affinity of this interaction remains unknown (Kadlec et al. 2004). Therefore, we carried out fluorescence anisotropy assays of $UPF2_S$ with 6-FAM-U_{12} RNA (Fig. 2B) and determined a dissociation constant (K_D) of ~600 nM, an order of magnitude higher than the K_D of apo-UPF1 for RNA (~50 nM) (Chakrabarti et al. 2011). Furthermore, an analytical SEC assay of $UPF2_S$ with the U_{15} RNA showed that it does not form a stable complex with RNA (Fig. 2C), which is consistent with the weak binding of $UPF2_S$ to RNA observed in EMSA (Supplemental Fig. 1C). Based on these observations, we hypothesize that the UPF2-mediated dissociation of UPF1 from RNA is unlikely to be a result of preferential binding of $UPF2_S$ to RNA, but is rather due to UPF2-induced conformational rearrangements and dynamics within UPF1 that destabilize the UPF1–RNA complex. This also explains the observation that addition of RNA led to disruption of a UPF1–UPF2 complex and that no stable ternary complex of UPF1, UPF2 and RNA could be isolated in vitro (Fig. 1C).

To test this hypothesis, we used a short construct of UPF2 (UPF2–U1BD, Fig. 1A) that spans the UPF1-binding region but lacks the MIF4G3 domain that was earlier shown to bind RNA (Kadlec et al. 2004). UPF2–U1BD has no appreciable affinity for RNA, precluding determination of a K_D for RNA binding by fluorescence anisotropy (Fig. 3A). Nevertheless, addition of increasing amounts of UPF2–U1BD to a mixture of UPF1 and 6-FAM-U_{12} RNA led to a steady decrease in fluorescence anisotropy, corresponding to a release of UPF1 from RNA (Fig. 3B). Conversely, addition of U_{15} RNA to a complex of UPF1 with UPF2–U1BD led to partial dissociation of the complex in analytical SEC, as indicated by the appearance of a peak corresponding to UPF1–U_{15} RNA (Supplemental Fig. 1D). It appears that UPF2–U1BD, without interacting with RNA, mediates the same effect as $UPF2_S$, substantiating the argument that the inability of UPF1 to concomitantly interact with UPF2 and RNA in a stable manner is not due to competition between the two proteins for RNA. To corroborate this observation, we tested the ability of a UPF2 construct lacking the carboxy-terminal MIF4G3 and UPF1-binding domains (UPF2-MIF4G1-2) to bind RNA and to displace UPF1 from RNA. We found that UPF2-MIF4G1-2 binds U_{12} RNA with an affinity comparable to that of $UPF2_S$ but unlike $UPF2_S$, it does not displace UPF1 from RNA (Fig. 3A,B). Correspondingly, RNA binding by $UPF1_{\Delta CH}$, a construct lacking the UPF2-interacting CH domain, remained unperturbed upon addition of $UPF2_S$ (Fig. 3C; Supplemental Fig. 2C).

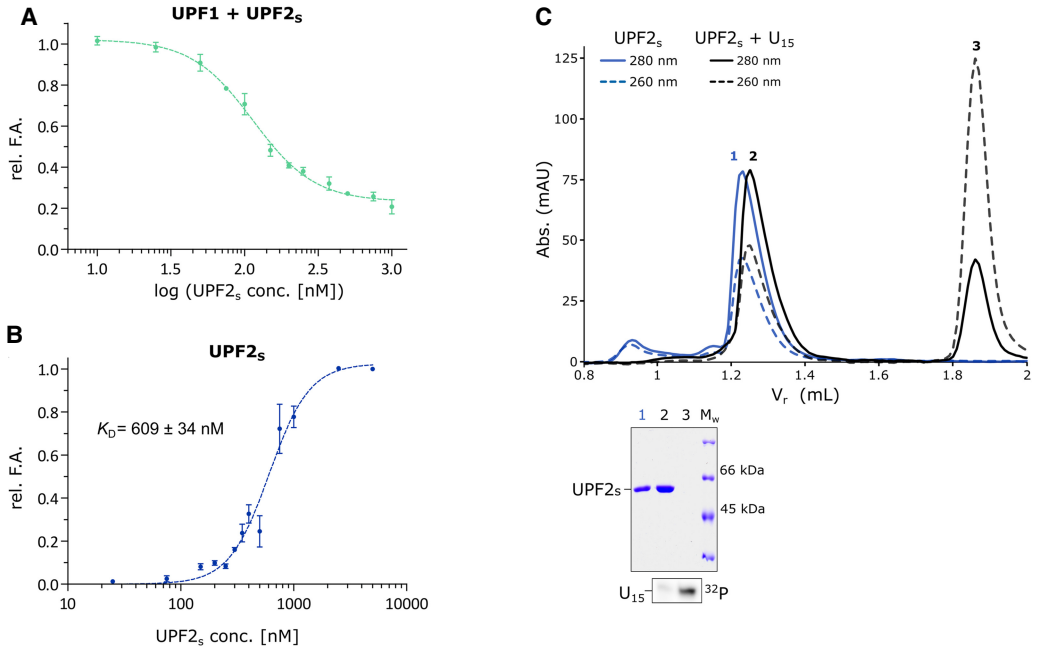

FIGURE 2. RNA-binding properties of UPF2$_S$ and its impact on binding of UPF1 to RNA. (*A*) Fluorescence anisotropy competition assay to determine how addition of UPF2$_S$ affects binding of UPF1 to 6-FAM-U$_{12}$ RNA. Titration of increasing amounts of UPF2$_S$ into a constant amount of UPF1–U$_{12}$ RNA mixture results in partial displacement of UPF1 from RNA. The data points and error bars of this and all other fluorescence anisotropy experiments are the mean and standard deviation of at least two independent experiments. (*B*) Fluorescence anisotropy assay to determine the dissociation constant (K_D) of the UPF2$_S$–U$_{12}$ RNA interaction. The error associated with the K_D is its standard deviation (SD). UPF2$_S$ binds U$_{12}$ RNA with a modest affinity, which is an order of magnitude lower than the RNA-binding affinity of UPF1 (~50 nM). (*C*) Analytical SEC analysis of binding of UPF2$_S$ to U$_{15}$ RNA. *Top* and *bottom* panels show the overlay of chromatograms of UPF2$_S$ without (blue traces) and with RNA (black traces), and the corresponding PAGE analyses of peak fractions of each run, respectively. Peak 3 at 1.9 mL corresponds to the U$_{15}$ RNA. UPF2$_S$ does not form a stable complex with RNA.

Helicases of the superfamily (SF) 1 bind RNA and ATP independently. Indeed, UPF1 has the highest binding affinity for RNA in the absence of any nucleotide. Although UPF1 does not undergo the drastic conformational change observed in DEAD-box helicases, it adopts a more compact form upon binding ATP and RNA, with the RecA domains positioned closer to each other compared to the apo state. The subtle conformational changes in the RecA domains during ATP binding and hydrolysis prompted us to test if nucleotide binding affects the UPF2-mediated release of UPF1 from RNA. To this end, we treated a preformed UPF1–UPF2$_S$ complex with equimolar U$_{15}$ RNA and an excess of a nonhydrolyzable ATP analog (ATPγS) and analyzed the protein–nucleotide mixture by analytical SEC (Fig. 3D). Addition of RNA dissociated the UPF1–UPF2$_S$ complex even in the presence of ATPγS, as indicated by appearance of the UPF1–RNA peak (Fig. 3D, peak 3 and corresponding PAGE analyses), while ATPγS alone did not disrupt the protein complex (Fig. 3D, peak 1 and corresponding PAGE analyses). We also analyzed the RNA-binding properties of a UPF1 mutant (UPF1$_{K498A}$), where the lysine residue of the Walker A motif (GXXGT/SG**K**T) was mutated to an alanine to abolish ATP binding (Walker et al. 1982; Fairman-Williams et al. 2010). The RNA-binding affinity of the mutant is comparable to that of wild-type UPF1 and titration of UPF2 into the UPF1$_{K498A}$–RNA mixture led to partial release of UPF1 from RNA, though not to the same extent as was observed for wild-type UPF1 (Supplemental Fig. 2C,D). Taken together, it appears that the effect of UPF2 on RNA binding by UPF1 does not depend on the nucleotide-bound state of the helicase and is independent of its catalytic activity. Based on the above, we conclude that dissociation of UPF1 from RNA upon addition of UPF2, and vice versa, stems from rearrangements in protein–protein/RNA interactions upon addition of the second binding partner and prevents formation of a stable ternary UPF1–UPF2–RNA complex. It is possible that a transient mRNP of UPF1, UPF2, and RNA is assembled in cells to rapidly activate UPF1, following which the complex is turned over to release UPF1 and UPF2 from RNA.

Conclusions

The NMD pathway involves the assembly and disassembly of several protein/RNA complexes to discern mRNA transcripts as bona fide substrates, and subsequently remodel mRNPs and completely degrade target mRNAs (Franks et al. 2010; Lee and Lykke-Andersen 2013, for reviews, see Karousis and Muhlemann 2019; Kishor et al. 2019;

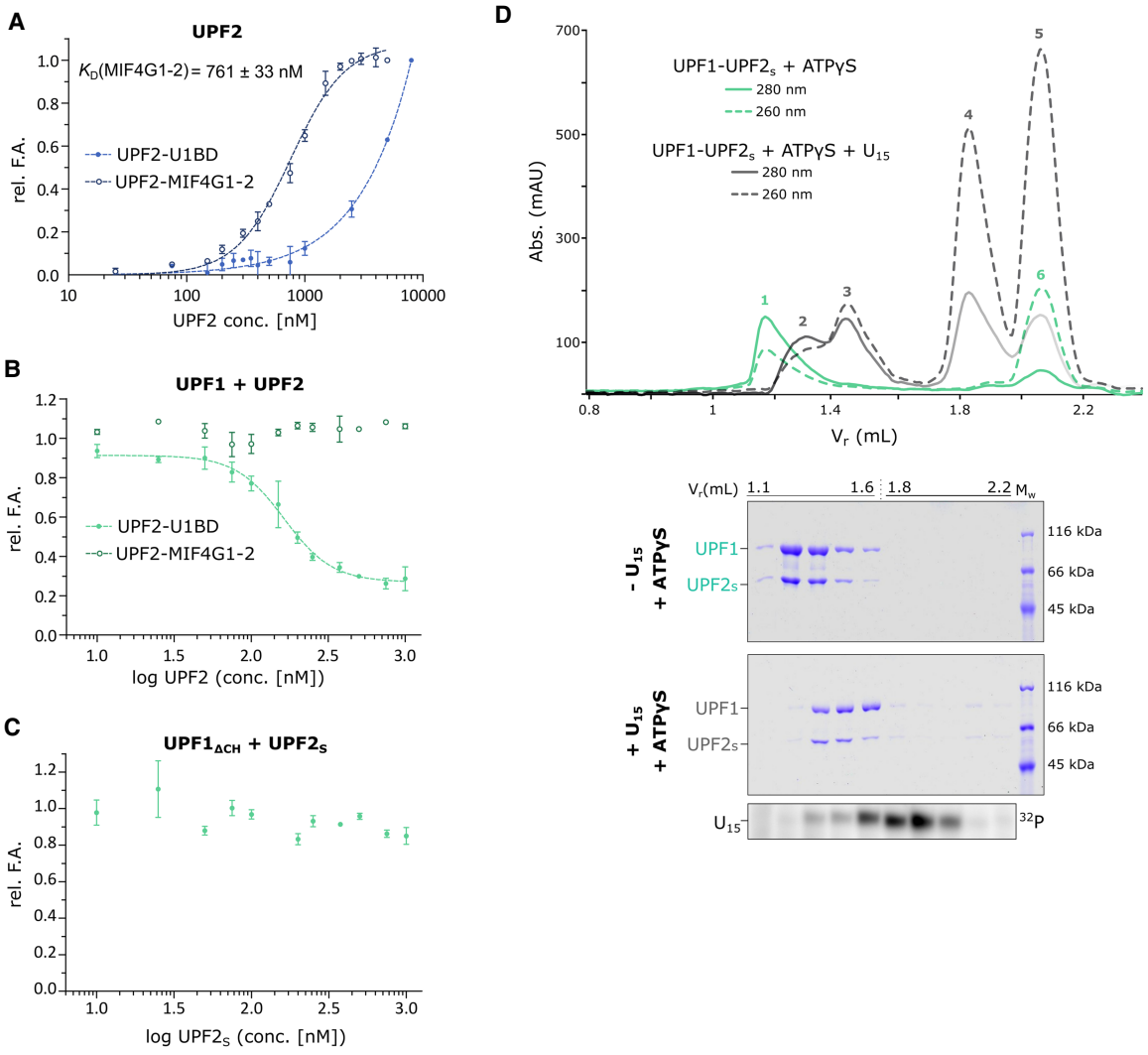

FIGURE 3. Displacement of UPF1 from RNA by UPF2 is not due to competition in RNA binding. (*A*) Quantitative measurements of RNA-binding affinities of UPF2 constructs comprising (UPF2–U1BD) and lacking the UPF1-binding site (UPF2-MIF4G1-2) by fluorescence anisotropy using 6-FAM-labeled U_{12} RNA. The K_D of UPF2-MIF4G1-2 is reported along with its SD. The affinity of UPF2-MIF4G1-2 (open circles) for RNA is comparable to that of $UPF2_S$, whereas UPF2–U1BD (filled circles) does not show any appreciable affinity for RNA. (*B*) Fluorescence anisotropy competition assays to determine the effect of UPF2–U1BD and UPF2-MIF4G1-2 on the UPF1–RNA interaction. The UPF2–U1BD protein that binds UPF1, but not RNA, is capable of displacing UPF1 from RNA (filled circles), whereas the MIF4G1-2 construct that binds RNA but lacks the UPF1-binding motif has no impact on RNA binding by UPF1 (open circles). (*C*) Fluorescence anisotropy competition assay of $UPF1_{\Delta CH}$ with $UPF2_S$. UPF2 has no effect on RNA binding by $UPF1_{\Delta CH}$, consistent with its inability to bind a UPF1 construct lacking the CH domain. (*D*) Analytical SEC analysis of a mixture of a UPF1–$UPF2_S$ complex, ATPγS and U_{15} RNA. (*Top*) Overlay of chromatograms of a mixture of the preformed UPF1–$UPF2_S$ complex and ATPγS, without (green traces) and with U_{15} RNA (black traces). (*Bottom*) SDS- and urea-PAGE analyses of consecutive SEC fractions in order of increasing retention volume, as indicated. Detection of U_{15} RNA is as described in Figure 1. Addition of RNA to UPF1–$UPF2_S$ leads to partial dissociation of the protein complex even in the presence of a nucleotide. The peaks between 1.8 and 2 mL correspond to excess U_{15} RNA and ATPγS.

Kurosaki et al. 2019). As a core component of the NMD pathway, UPF1 is involved in several of these complexes, often through transient interactions (Lavysh and Neu-Yilik 2020). Examples of UPF1-centric complexes in NMD are the SURF (SMG1–UPF1–eRFs) complex (assembled on the PTC-stalled ribosome) and the decay-inducing (DECID) complex (formed upon association of SURF with UPF2-3-bound EJC) (Yamashita et al. 2001; Kashima et al. 2006). Additionally, both phosphorylated and unphosphorylated UPF1 interact with the endonuclease SMG6 and phosphorylated UPF1 also engages the SMG5/SMG7 heterodimer, which in turn bridges the target mRNP to the deadenylation machinery (Okada-Katsuhata et al. 2012; Loh et al. 2013; Chakrabarti et al. 2014; Nicholson et al. 2014). The involvement of SMG6 in NMD depends both on UPF1 as well as binding of SMG5/SMG7 to phospho-UPF1, indicating a complex interplay of interactions at work (Boehm et al. 2021). It therefore appears intuitive that many of these

interactions must be short-lived to facilitate progression of NMD and efficient degradation of the nonsense mRNA.

In this study, we show that UPF1 is unable to engage UPF2 and RNA simultaneously to form a stable ternary complex. We investigate this in detail and provide an underlying mechanism for our observations and that of Chamieh and coworkers, where binding of UPF1 to RNA was weakened in the presence of UPF2. These observations are somewhat counterintuitive to our understanding of the stimulation of UPF1's helicase and RNA-dependent ATPase activities by UPF2. As the helicase has a low basal catalytic activity in vitro in the absence of its binding partners, one role of UPF2 might be to activate UPF1 for its function in NMD and other decay pathways. It is widely speculated that activation of UPF1 during NMD occurs in the context of the EJC–UPF3-2-1 complex. The cryo-EM structure of the EJC–UPF complex shows UPF1 positioned toward the 3′-end of the EJC-bound RNA, poised to translocate in the 5′–3′ direction (Melero et al. 2012). However, it is not clear from structural and biochemical studies whether activation of UPF1 occurs early on in the NMD pathway (immediately after association with EJC–UPF3-2) or at a later stage, just prior to degradation. It is possible that association of UPF1 with the EJC–UPF3-2 complex leads to its activation as well as dissociation from the mRNA, while still being tethered to the mRNP via protein–protein interactions. Once activated UPF1 rebinds the mRNA, it would dissociate from the EJC–UPF3-2 complex and translocate along the mRNA toward its 3′-end. Alternatively, EJC-independent UPF2 could bind UPF1, activate it and dissociate from UPF1 rapidly, leaving it free to rebind the mRNA. This raises the question of how UPF2 is recruited to the nonsense-mRNP independent of the EJC. We present evidence for binding of UPF2 to RNA with a modest affinity, although this interaction is not as stable as that of UPF1 with RNA. It is not known if UPF2 associates with other NMD components, apart from UPF1 and UPF3. The ATPase-mediated dissociation of UPF1 from RNA has been shown to be important for cellular control of NMD specificity (Chapman et al. 2022). It is possible that the primary role of UPF2 in NMD is to facilitate release of UPF1 from RNA, while activating it at the same time. This implies that a transient complex of UPF1, UPF2, and RNA, which is not captured in our equilibrium binding studies, must be assembled during this step. Rapid dissociation of the transient UPF1–UPF2–RNA complex would also allow free UPF2, which is significantly less abundant than UPF1, to bind and activate another RNA-bound UPF1 molecule.

Recent studies on another UPF1-mediated decay pathway, Staufen-mediated mRNA decay (SMD) showed the involvement of UPF2, where it acts as an adaptor between UPF1 and the double-stranded (ds) RNA-binding protein Stau1 and activates UPF1 within this complex (Gowravaram et al. 2019). Although the ability of the UPF1–UPF2–Stau1 complex to interact with dsRNA has been shown in this study, it would be worthwhile to investigate if the protein complex can stably associate with dsRNA and if UPF2 also affects the RNA-binding properties of Stau1. How UPF1 activation by UPF2 is achieved in the various decay pathways while keeping the helicase associated with the target mRNP remains a conundrum that requires further investigation.

MATERIALS AND METHODS

Protein expression and purification

All human UPF1 and UPF2 constructs and mutant proteins used in this study were expressed as 6×-His or His-Thioredoxin (Trx) fusions in *Escherichia coli* BL21 (*DE3*) STAR pRARE cells at 18°C for at least 15 h. Cells expressing recombinant proteins were lysed using lysis buffer (50 mM Tris-HCl pH 7.5, 500 mM NaCl, 10% glycerol, 1 mM $MgCl_2$, 1 µM $ZnCl_2$, 0.1 M urea, and 10 mM imidazole), supplemented with protease inhibitors (1 mM PMSF) and DNase I. The proteins were isolated from the crude lysate by Ni^{2+}-affinity chromatography and washed successively with lysis buffer, chaperone wash buffer (50 mM Tris-HCl pH 7.5, 1 M NaCl, 10% glycerol, 10 mM $MgCl_2$, 50 mM KCl, 1 µM $ZnCl_2$, 2 mM ATP, and 10 mM imidazole) and low salt wash buffer (50 mM Tris-HCl pH 7.5, 150 mM NaCl, 10% glycerol, 1 mM $MgCl_2$, 1 µM $ZnCl_2$, and 10 mM imidazole) gradually. Finally, target proteins were eluted with nickel column elution buffer (50 mM Tris-HCl pH 7.5, 150 mM NaCl, 10% glycerol, 1 mM $MgCl_2$, 1 µM $ZnCl_2$, and 300 mM imidazole). The affinity tags on UPF1 and UPF2 constructs were not removed. UPF1 (wild-type and the K498A mutant), $UPF1_{\Delta CH}$, $UPF2_L$, and $UPF2_S$ were subjected to a further purification step using a HiTrap Heparin Sepharose HP column (GE Healthcare) and heparin buffers A (20 mM Tris-HCl pH 7.5, 10% glycerol, 1 mM $MgCl_2$, 1 µM $ZnCl_2$, and 2 mM DTT) and B (20 mM Tris-HCl pH 7.5, 1 M NaCl, 10% glycerol, 1 mM $MgCl_2$, 1 µM $ZnCl_2$, and 2 mM DTT). Proteins were eluted from the column using a linear concentration gradient of NaCl. All proteins including UPF2–U1BD were purified by a final size-exclusion chromatography step (using Superdex 75 or Superdex 200 columns, GE Healthcare) in SEC buffer (20 mM Tris-HCl pH 7.5, 150 mM NaCl, 5% glycerol, 1 mM $MgCl_2$, 1 µM $ZnCl_2$, and 2 mM DTT).

Complexes of UPF1 and various UPF2 constructs were formed by mixing together the two proteins in a 1:1.2 molar ratio (with UPF1 in excess) overnight at 4°C, followed by SEC on a Superdex 200 column.

Analytical SEC

An amount of 700 pmol of the single proteins (UPF1 or UPF2 alone), UPF1–UPF2 complexes or the mixtures of approximately equimolar amounts of UPF1 and UPF2 were mixed with 700 pmol of a 15-mer poly(U)-RNA (U_{15}) (Eurofins Genomics) to a final volume of 50 µL in A-SEC buffer (20 mM HEPES pH 7.5, 100 mM NaCl, 5% glycerol, 1 mM $MgCl_2$, 1 µM $ZnCl_2$, 2 mM DTT) and incubated on ice overnight. Wherever mentioned, 7 nmol of ATPγS was added to SEC mixture. Individual proteins and protein–RNA complexes were resolved on a Superdex 200 Increase 3.2/300

column (GE Healthcare). The peak fractions were analyzed by SDS-PAGE, followed by staining with Coomassie brilliant blue. Peak fractions for analytical SEC runs performed with U_{15} RNA were radiolabeled with [γ-^{32}P]-ATP, as described below and visualized on 15% urea-PAGE by autoradiography. The curves of chromatograms in the same figure were normalized manually for intuitive comparison.

Sample labeling and electrophoretic mobility shift assays

A total of 2 µL of peak fractions from indicated SEC runs was treated with [γ-^{32}P]-ATP (Hartmann Analytic GmbH) and T4 polynucleotide kinase (Molox GmbH) in PNK A buffer (Thermo Fisher) for 1.5 h at 37°C in order to 5′-end label the U_{15} RNA therein. Excess [γ-^{32}P]-ATP was separated from the labeled RNA by purification on a G25 spin column (GE HealthCare).

For electrophoretic mobility shift assays (EMSA), 10 pmol U_{15} RNA (Eurofins Genomics) was radiolabeled at the 5′-end with [γ-^{32}P]-ATP and subsequently purified as described above. An amount of 0.2 pmol of radiolabeled RNA was incubated with 150 nM UPF1, 150 nM UPF2 or a preformed UPF1–UPF2 in assembly buffer (20 mM HEPES, 100 mM NaCl, 0.1% NP-40, 0.5% Glycerol, 1 mM DTT, 0.5 mM EDTA) in a total volume of 10 µL for 30 min on ice. Samples were resolved on a 5% native PAGE that was run at 160 V for 2.5 h at 4°C. Bands containing RNA were visualized via autoradiography using a phosphor-imager (GE Healthcare).

Native gel analysis

A UPF1–U_{15} RNA complex was formed on a preparative scale by mixing 100 µg UPF1 protein with a 1.2-fold molar excess of fluorescein-labeled U_{15} RNA, followed by size-exclusion chromatography on a 2.4 mL Superdex 200 column. The peak fraction containing both UPF1 and U_{15} RNA was used for the native gel analysis. An amount of 2 µg of individual proteins and 4 µg of complexes were used in each case. Proteins were mixed with a 1.2-fold molar excess of fluorescein-labeled U_{15} RNA and incubated at room temperature for 30 min. Thereafter, samples were reconstituted in native gel sample buffer and directly analyzed on a 4%–20% Tris-Glycine native gel (Thermo Fisher Scientific). Proteins were visualized by staining with Coomassie brilliant blue and the U_{15} RNA was detected by fluorescence scanning using a Typhoon scanner (GE Healthcare).

Fluorescence anisotropy

To determine the affinity of UPF2 constructs for RNA, 10 nM of a 12-mer poly(U)-RNA (U_{12}) labeled with 6-FAM at its 5′-end was mixed with increasing concentrations of human $UPF2_S$, UPF2–MIF4G1-2, and UPF2–U1BD in FA-binding buffer (20 mM HEPES pH 7.5, 100 mM NaCl, 1 mM $MgCl_2$, 100 µg/mL BSA) for 30 min at room temperature. An amount of 40 µL of each sample was transferred to a black 384-well plate (PerkinElmer OptiPlate 384-F) and fluorescence polarization was measured with a Tecan Spark plate reader at 25°C. The reading obtained in the absence of UPF2 (RNA alone sample) was considered as background and subtracted from all fluorescence polarization (FP) values. Fluorescence anisotropy was calculated from fluorescence polarization using the formula 2·FP/(3-FP) and normalized against the value obtained for the highest UPF2 concentration. The data shown are an average of at least two independent experiments and were fitted to an equation representing one site—specific binding with Hill slope in GraphPad Prism 5.00. Error bars and the error associated with the reported K_D denote standard deviation (SD).

In order to determine the effect of different UPF2 constructs on RNA binding of UPF1, 70 nM hUPF1 and 10 nM of 6-FAM-labeled U_{12} RNA were mixed with increasing concentrations of human $UPF2_S$, UPF2-MIF4G1-2, and UPF2-U1BD in FA-binding buffer for 30 min at room temperature. The fluorescence anisotropy competition experiment of UPF1 with $UPF2_S$ at pH 6.5 was performed using $FA_{6.5}$-binding buffer (50 mM MES pH 6.5, 100 mM NaCl, 1 mM $MgCl_2$, 100 µg/mL BSA). Fluorescence polarization was recorded and fluorescence anisotropy was calculated as described above. The data, an average of three independent experiments (except for UPF2-MIF4G1-2, where only two independent experiments were performed), were fitted, when possible, to an equation describing dose-dependent inhibition [log(inhibitor) versus response—variable slope] in GraphPad Prism 5.00. As above, data points and error bars represent the mean and standard deviation of three independent experiments.

DATA DEPOSITION

All data for this manuscript are contained within the main article and Supplemental Information.

SUPPLEMENTAL MATERIAL

Supplemental material is available for this article.

ACKNOWLEDGMENTS

We thank Elena Conti for support at the initial stage of this project, Markus Wahl for the gift of 6-FAM-labeled U_{12} RNA, and Juliane Metzke for purification of the UPF2-MIF4G1-2 protein. Access to the Tecan Spark plate reader was provided by the core facility BioSupraFAB (Freie Universität Berlin) supported by the DFG. This study was supported by the Priority Programme SPP 1935 of the Deutsche Forschungsgemeinschaft (CH1245/3-1 and CH1245/3-2 to S.C.) as well as the DFG research grant CH1245/6-1 to S.C. S.C. acknowledges the support of the Heisenberg Programme of the DFG (CH 1245/5-1).

Author contributions: S.C.: conceptualization, funding acquisition, supervision; G.X.: protein purification, SEC analysis, ATPase assays, fluorescence anisotropy; V.M. and M.P.: fluorescence anisotropy; A.A. and M.P.: EMSAs; U.J.: native PAGE analysis; A.A. and S.C.: writing—original draft; all authors: writing—review and editing.

Received March 28, 2022; accepted November 6, 2022.

REFERENCES

Boehm V, Kueckelmann S, Gerbracht JV, Kallabis S, Britto-Borges T, Altmuller J, Kruger M, Dieterich C, Gehring NH. 2021. SMG5-SMG7 authorize nonsense-mediated mRNA decay by enabling SMG6 endonucleolytic activity. *Nat Commun* **12:** 3965. doi:10.1038/s41467-021-24046-3

Bourgeois CF, Mortreux F, Auboeuf D. 2016. The multiple functions of RNA helicases as drivers and regulators of gene expression. *Nat Rev Mol Cell Biol* **17:** 426–438. doi:10.1038/nrm.2016.50

Buchwald G, Ebert J, Basquin C, Sauliere J, Jayachandran U, Bono F, Le Hir H, Conti E. 2010. Insights into the recruitment of the NMD machinery from the crystal structure of a core EJC-UPF3b complex. *Proc Natl Acad Sci* **107:** 10050–10055. doi:10.1073/pnas.1000993107

Chakrabarti S, Jayachandran U, Bonneau F, Fiorini F, Basquin C, Domcke S, Le Hir H, Conti E. 2011. Molecular mechanisms for the RNA-dependent ATPase activity of Upf1 and its regulation by Upf2. *Mol Cell* **41:** 693–703. doi:10.1016/j.molcel.2011.02.010

Chakrabarti S, Bonneau F, Schussler S, Eppinger E, Conti E. 2014. Phospho-dependent and phospho-independent interactions of the helicase UPF1 with the NMD factors SMG5-SMG7 and SMG6. *Nucleic Acids Res* **42:** 9447–9460. doi:10.1093/nar/gku578

Chamieh H, Ballut L, Bonneau F, Le Hir H. 2008. NMD factors UPF2 and UPF3 bridge UPF1 to the exon junction complex and stimulate its RNA helicase activity. *Nat Struct Mol Biol* **15:** 85–93. doi:10.1038/nsmb1330

Chapman JH, Craig JM, Wang CD, Gundlach JH, Neuman KC, Hogg JR. 2022. UPF1 mutants with intact ATPase but deficient helicase activities promote efficient nonsense-mediated mRNA decay. *Nucleic Acids Res* **50:** 11876–11894. doi:10.1093/nar/gkac1026

Cheng Z, Muhlrad D, Lim MK, Parker R, Song H. 2007. Structural and functional insights into the human Upf1 helicase core. *EMBO J* **26:** 253–264. doi:10.1038/sj.emboj.7601464

Cho NH, Cheveralls KC, Brunner AD, Kim K, Michaelis AC, Raghavan P, Kobayashi H, Savy L, Li JY, Canaj H, et al. 2022. OpenCell: endogenous tagging for the cartography of human cellular organization. *Science* **375:** eabi6983. doi:10.1126/science.abi6983

Clerici M, Mourao A, Gutsche I, Gehring NH, Hentze MW, Kulozik A, Kadlec J, Sattler M, Cusack S. 2009. Unusual bipartite mode of interaction between the nonsense-mediated decay factors, UPF1 and UPF2. *EMBO J* **28:** 2293–2306. doi:10.1038/emboj.2009.175

Clerici M, Deniaud A, Boehm V, Gehring NH, Schaffitzel C, Cusack S. 2014. Structural and functional analysis of the three MIF4G domains of nonsense-mediated decay factor UPF2. *Nucleic Acids Res* **42:** 2673–2686. doi:10.1093/nar/gkt1197

Fairman-Williams ME, Guenther UP, Jankowsky E. 2010. SF1 and SF2 helicases: family matters. *Curr Opin Struct Biol* **20:** 313–324. doi:10.1016/j.sbi.2010.03.011

Franks TM, Singh G, Lykke-Andersen J. 2010. Upf1 ATPase-dependent mRNP disassembly is required for completion of nonsense-mediated mRNA decay. *Cell* **143:** 938–950. doi:10.1016/j.cell.2010.11.043

Gehring NH, Wahle E, Fischer U. 2017. Deciphering the mRNP code: RNA-bound determinants of post-transcriptional gene regulation. *Trends Biochem Sci* **42:** 369–382. doi:10.1016/j.tibs.2017.02.004

Gowravaram M, Schwarz J, Khilji SK, Urlaub H, Chakrabarti S. 2019. Insights into the assembly and architecture of a Staufen-mediated mRNA decay (SMD)-competent mRNP. *Nat Commun* **10:** 5054. doi:10.1038/s41467-019-13080-x

Hein MY, Hubner NC, Poser I, Cox J, Nagaraj N, Toyoda Y, Gak IA, Weisswange I, Mansfeld J, Buchholz F, et al. 2015. A human interactome in three quantitative dimensions organized by stoichiometries and abundances. *Cell* **163:** 712–723. doi:10.1016/j.cell.2015.09.053

Kadlec J, Izaurralde E, Cusack S. 2004. The structural basis for the interaction between nonsense-mediated mRNA decay factors UPF2 and UPF3. *Nat Struct Mol Biol* **11:** 330–337. doi:10.1038/nsmb741

Karousis ED, Muhlemann O. 2019. Nonsense-mediated mRNA decay begins where translation ends. *Cold Spring Harb Perspect Biol* **11:** a032862. doi:10.1101/cshperspect.a032862

Kashima I, Yamashita A, Izumi N, Kataoka N, Morishita R, Hoshino S, Ohno M, Dreyfuss G, Ohno S. 2006. Binding of a novel SMG-1-Upf1-eRF1-eRF3 complex (SURF) to the exon junction complex triggers Upf1 phosphorylation and nonsense-mediated mRNA decay. *Genes Dev* **20:** 355–367. doi:10.1101/gad.1389006

Kishor A, Fritz SE, Hogg JR. 2019. Nonsense-mediated mRNA decay: the challenge of telling right from wrong in a complex transcriptome. *Wiley Interdiscip Rev RNA* **10:** e1548. doi:10.1002/wrna.1548

Kurosaki T, Popp MW, Maquat LE. 2019. Quality and quantity control of gene expression by nonsense-mediated mRNA decay. *Nat Rev Mol Cell Biol* **20:** 406–420. doi:10.1038/s41580-019-0126-2

Lavysh D, Neu-Yilik G. 2020. UPF1-mediated RNA decay—danse macabre in a cloud. *Biomolecules* **10:** 999. doi:10.3390/biom10070999

Lee SR, Lykke-Andersen J. 2013. Emerging roles for ribonucleoprotein modification and remodeling in controlling RNA fate. *Trends Cell Biol* **23:** 504–510. doi:10.1016/j.tcb.2013.05.001

Lee SR, Pratt GA, Martinez FJ, Yeo GW, Lykke-Andersen J. 2015. Target discrimination in nonsense-mediated mRNA decay requires Upf1 ATPase activity. *Mol Cell* **59:** 413–425. doi:10.1016/j.molcel.2015.06.036

Leeds P, Peltz SW, Jacobson A, Culbertson MR. 1991. The product of the yeast UPF1 gene is required for rapid turnover of mRNAs containing a premature translational termination codon. *Genes Dev* **5:** 2303–2314. doi:10.1101/gad.5.12a.2303

Linder P, Jankowsky E. 2011. From unwinding to clamping—the DEAD box RNA helicase family. *Nat Rev Mol Cell Biol* **12:** 505–516. doi:10.1038/nrm3154

Loh B, Jonas S, Izaurralde E. 2013. The SMG5-SMG7 heterodimer directly recruits the CCR4-NOT deadenylase complex to mRNAs containing nonsense codons via interaction with POP2. *Genes Dev* **27:** 2125–2138. doi:10.1101/gad.226951.113

Lopez-Perrote A, Castano R, Melero R, Zamarro T, Kurosawa H, Ohnishi T, Uchiyama A, Aoyagi K, Buchwald G, Kataoka N, et al. 2016. Human nonsense-mediated mRNA decay factor UPF2 interacts directly with eRF3 and the SURF complex. *Nucleic Acids Res* **44:** 1909–1923. doi:10.1093/nar/gkv1527

Machado de Amorim A, Chakrabarti S. 2021. Assembly of multicomponent machines in RNA metabolism: a common theme in mRNA decay pathways. *Wiley Interdiscip Rev RNA* **13:** e1684. doi:10.1002/wrna.1684

Melero R, Buchwald G, Castano R, Raabe M, Gil D, Lazaro M, Urlaub H, Conti E, Llorca O. 2012. The cryo-EM structure of the UPF-EJC complex shows UPF1 poised toward the RNA 3′ end. *Nat Struct Mol Biol* **19:** 498–505. doi:10.1038/nsmb.2287

Nicholson P, Josi C, Kurosawa H, Yamashita A, Muhlemann O. 2014. A novel phosphorylation-independent interaction between SMG6 and UPF1 is essential for human NMD. *Nucleic Acids Res* **42:** 9217–9235. doi:10.1093/nar/gku645

Ohnishi T, Yamashita A, Kashima I, Schell T, Anders KR, Grimson A, Hachiya T, Hentze MW, Anderson P, Ohno S. 2003.

Phosphorylation of hUPF1 induces formation of mRNA surveillance complexes containing hSMG-5 and hSMG-7. *Mol Cell* **12:** 1187–1200. doi:10.1016/S1097-2765(03)00443-X

Okada-Katsuhata Y, Yamashita A, Kutsuzawa K, Izumi N, Hirahara F, Ohno S. 2012. N- and C-terminal Upf1 phosphorylations create binding platforms for SMG-6 and SMG-5:SMG-7 during NMD. *Nucleic Acids Res* **40:** 1251–1266. doi:10.1093/nar/gkr791

Walker JE, Saraste M, Runswick MJ, Gay NJ. 1982. Distantly related sequences in the α- and β-subunits of ATP synthase, myosin, kinases and other ATP-requiring enzymes and a common nucleotide binding fold. *EMBO J* **1:** 945–951. doi:10.1002/j.1460-2075.1982.tb01276.x

Yamashita A, Ohnishi T, Kashima I, Taya Y, Ohno S. 2001. Human SMG-1, a novel phosphatidylinositol 3-kinase-related protein kinase, associates with components of the mRNA surveillance complex and is involved in the regulation of nonsense-mediated mRNA decay. *Genes Dev* **15:** 2215–2228. doi:10.1101/gad.913001

MEET THE FIRST AUTHOR

Guangpu Xue

***Meet the First Author(s)* is an editorial feature within *RNA*, in which the first author(s) of research-based papers in each issue have the opportunity to introduce themselves and their work to readers of *RNA* and the RNA research community. Guangpu Xue is the first author of this paper, "Modulation of RNA-binding properties of the RNA helicase UPF1 by its activator UPF2." Guangpu obtained a bachelor's degree and a master's degree in China, and is currently a PhD candidate at the Freie Universität Berlin.**

What are the major results described in your paper and how do they impact this branch of the field?

In this paper, we show that the RNA helicase UPF1, its activator UPF2, and RNA cannot form a stable ternary complex, which is somewhat surprising and counterintuitive. We show that dissociation of the UPF1–RNA complex by UPF2 is not a consequence of direct competition in RNA binding but rather an allosteric effect that is likely mediated by the conformational changes in UPF1 that are induced upon UPF2 binding. Our studies highlight the transient nature of the mRNP assembled during UPF1 activation. We speculate that dynamic assembly and disassembly of mRNPs is probably a common and recurring theme in many mRNA processing pathways.

What led you to study RNA or this aspect of RNA science?

My research interest during my master's study was structural biology. After graduating from my master's program, I worked as a research assistant in my former lab while continuing to seek an opportunity with my PhD Professor Sutapa Chakrabarti, who advertised an open position in 2018. I contacted her and found the research in her lab to be quite interesting. The lab investigates pathways of mRNA decay to determine how the mRNPs connect to the mRNA degradation machinery using a structural biochemistry approach. I think this research will reveal deeper insights into the regulation of gene expression, which helps us to better understand physiological and pathological processes in eukaryotes.

What are some of the landmark moments that provoked your interest in science or your development as a scientist?

Being a scientist has been my dream since I was a child. Although biochemistry was not my favorite subject, it was the one assigned to me in college, and I found it more and more interesting as I learned more and more about it. I experienced some setbacks during my studies, which led me to take a more circuitous route through my early career than many of my peers. I got the offer of my current PhD position after 1.5 years of short-term work. I might be slow and my path might be hard, but I am always on the right track and will hold my own.

If you were able to give one piece of advice to your younger self, what would that be?

Do not be discouraged by current obstacles; things will take a turn for the better if you go on learning, and you will succeed eventually.

Are there specific individuals or groups who have influenced your philosophy or approach to science?

Professor Xiaojun Hu (Linyi University) played an enlightening role in my scientific career. She supervised my bachelor's thesis and taught me basic experimental skills and scientific thinking. Professors Mingdong Huang (Fuzhou University) and Sutapa Chakrabarti (Freie Universität Berlin) are my master's and PhD supervisors; they are really nice people who have patience and are well equipped with professional knowledge. They have given me a lot of encouragement and support, which strengthened my pathway to a scientific career.